TERAHERTZ LASERS

PACS numbers: 73.21.Cd; 72.20.Ht; 72.30.+q; 78.67.Pt
DOI: 10.1070/QE2010v040n05ABEH014298

Amplification of terahertz radiation on transitions between Wannier – Stark ladders in weak-barrier superlattices

A.A. Andronov, E.P. Dodin, D.I. Zinchenko, Yu.N. Nozdrin, A.A. Marmalyuk, A.A. Padalitsa

Abstract. **The experimental and numerical studies of the transport properties and wave functions of electrons in GaAs/$Al_xGa_{1-x}As$ superlattices with weak barriers in a strong electric field demonstrate the possibility of terahertz lasing on transitions between Wannier – Stark ladders, which can be tuned by applying voltage. The calculated gain can be as high as 500 cm^{-1}, which exceeds several times the values characteristic of modern THz quantum cascade lasers. Thus, one would expect lasing to occur in a simple n^+ – superlattice – n^+ stripe structure. Such lasers, due to the possibility of wide tuning and simplicity of the superlattices they are based on, could compete with cascade lasers.**

Keywords: *semiconductor superlattices, Wannier – Stark levels, population inversion, negative differential conductivity, stimulated electromagnetic emission, terahertz range, gain, stripe cavity loss, lasing*.

1. Introduction

In 1971 – 1972 Kazarinov and Suris [1, 2] proposed a laser design based on intraband transitions in quantum wells of semiconductor superlattices (SLs) [3]. Two mechanisms of population inversion between the levels in wells were discussed. In the first, which can be referred to as *injection* mechanism (Fig. 1, region 3), the electrons tunnel (due to the applied voltage) from the lower level of some well to the upper (third) level of a neighbouring well. As a result, the third and second levels in the wells may undergo population inversion. In the second (*universal*) mechanism (region 2), an applied voltage lowers the upper (e.g., second) level in a neighbouring well below the first (ground) level in the starting well. Due to this, at a quasi-equilibrium distribution of electrons over well levels, population inversion arises between these levels. An important feature of the second mechanism is the change in the transition frequency with a change in voltage, which allows one to design a laser with a voltage controlled frequency.

A.A. Andronov, E.P. Dodin, D.I. Zinchenko, Yu.N. Nozdrin Institute for Physics of Microstructures, Russian Academy of Sciences, ul. Ul'yanova 46, 603950 Nizhnii Novgorod, Russia; e-mail: andron@ipm.sci-nnov.ru, dodin@ipm.sci-nnov.ru, dimazzz80@mail.ru, nozdrin@ipm.sci-nnov.ru; **A.A. Marmalyuk, A.A. Padalitsa** SIGMA PLUS Ltd., ul. Vvedenskogo 3, 117342 Moscow, Russia

Received 19 February 2010
Kvantovaya Elektronika **40** (4) 400 – 405 (2010)
Translated by Yu.P. Sin'kov

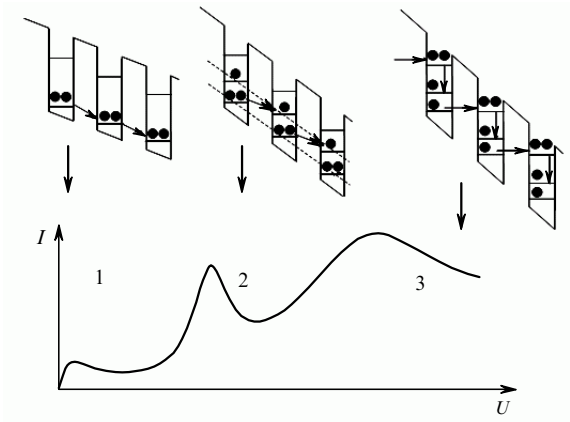

Figure 1. $I - U$ characteristic, NDC, and the mechanisms of level population inversion: (1) Esaki – Tsu NDC [3] (no inversion between the levels); (2) interwell inversion between the first and second Wannier – Stark ladders; and (3) intrawell inversion.

Kazarinov and Suris considered SLs with weakly coupled quantum wells (i.e., SLs with '*strong*' barriers). In this case, the mechanisms of population inversion proposed in [1, 2] have an inherent drawback (which was also evident for the authors): inversion arises in the range of static negative differential conductivity (NDC) of the current – voltage ($I - U$) characteristic of the SL [Fig. 1, region 3 in the dependence $I(U)$]. The negative differential conductivity arises because the distance between the energy levels in the neighbouring wells increases with an increase in the field; accordingly, the transition probability to this level decreases, and the current drops. Static NDC makes the electric field distribution in the SL nonuniform, thus hindering the design of such lasers.

Only after two decades Faist et al. [4] proposed to replace a simple SL by an SL with a complex period, i.e., by cascades with a relaxation region between wells, where the static NDC is suppressed. But the injection mechanism of inversion is retained. Thus, quantum cascade lasers were designed, first in the mid-IR range [4] and then in the THz range [5]. The next 15 years of the studies devoted to cascade lasers (see, for example, [6]) have brought significant achievements in this field. Various possible schemes of such lasers have been analysed. Modern cascade lasers can operate at almost any wavelength in the range of 3 – 200 μm; nevertheless, their tuning range is rather narrow.

Here, we return to the universal lasing mechanism, corresponding to the transport in simple SLs. As will be shown below, in the case of transport in weak-barrier SLs,

the static NDC is either suppressed or is absent at all, due to which this mechanism becomes efficient.

We investigated several SLs based on $GaAs/Al_xGa_{1-x}As$ heterostructures grown by metal organic chemical vapor deposition (MOCVD), with weak barriers, where the Al content x was 10 % – 15 % (see also [7–9]). We report the results for two SLs: SL426 and SL816 (Table 1). For the effects under consideration, it is not the barrier structure that plays a key role but its 'strength' – product of the barrier width by the Al content. Therefore, we refer to these barriers as weak rather than narrow. They can be described by a δ-function potential; using MOCVD, one can obtain such barriers of satisfactory quality.

Table 1.

CP	ε_0/ meV	$\Delta\varepsilon_1$/ meV	ε_1/ meV	ε_{gap}/ meV	ε_2/ meV	$\Delta\varepsilon_2$/ meV	$d = w+b$/ Å	N	F_t/ kV cm^{-1}
426	3.2	11.2	14.4	7.1	21.3	34.9	185 + 10	100	3.3
816	7.4	9.8	17.2	16.8	33.9	32.5	160 + 20	1000	24.3

Note: ε_0 and ε_1 are, respectively, the bottom and top of the first miniband; $\Delta\varepsilon_1$ is the width of the first miniband; ε_{gap} is the width of the first forbidden miniband; ε_2 and $\Delta\varepsilon_2$ are, respectively, the bottom and width of the second miniband; F_t is the characteristic electric field of tunneling through the first forbidden miniband; and N is the number of periods.

The initial motivation for studying the transport in weak-barrier SLs was to implement the conditions under which the ascending (due to the strong interminiband tunneling, caused by the barrier weakness) portion of the $I-U$ characteristic (without static NDC) exhibits dynamic NDC in the THz range near the Bloch frequency $\Omega = eFd/\hbar$ (e is the elementary charge, F is the electric field, and d is the SL period) [10]. Within the quantum-well band diagram in Fig. 1, the mechanism of dynamic NDC, as well as the Esaki–Tsu NDC [3], corresponds to the transition between Wannier–Stark levels within the same ladder. The Wannier–Stark levels are the result of transformation of the quantum-well levels under electric field. We can roughly consider them as energy-shifted by a value corresponding to the potential drop between the wells (Fig. 1). The levels within one ladder are equally occupied: all the wells are equivalent in a homogeneous field. Therefore, the THz dynamic NDC that was discussed in [10], as well as the static NDC [3] (Fig. 1, case 1) lacks global inversion; its value is comparable with the static NDC. Concerning the transitions within the same Wannier–Stark ladder, population inversion arises only in indirect transitions with a change in momentum along the SL wells, with allowance for scattering [11]. The Wannier–Stark levels belonging to different ladders, whose energies correspond to different SL levels (minibands) i (for example, $i = 1$ and 2),

$$E_{i,l} = \varepsilon_i \pm l\hbar\Omega = \varepsilon_i \pm leFd \tag{1}$$

(where $l = 0, 1, 2, \ldots$ is the well number), are occupied differently. Therefore, inversion can be implemented between these ladders. There is an optical transition between the ladders, and thus conventional lasing may occur. The NDC value and electromagnetic radiation gain on this transition can be significant, because, due to the weak barriers, the wave functions are delocalised at ladders, and the interladder transition matrix element (corresponding to the transitions between different levels of different wells) can be large in the case of a significant change in the well number ($l = 2, 3, \ldots$). The transition frequency ω is tuned by an applied electric field F in the same way as the Bloch frequency $\Omega = eFd/\hbar$: $\omega = (\varepsilon_i - \varepsilon_j)/\hbar \pm \Delta l\Omega$. Here, ε_i and ε_j are the energy levels of different ladders ($i \neq j$) and Δl is the change in the well number at the optical transition ($\Delta l = 2, 3, \ldots$).

2. $I-U$ characteristics of weak-barrier superlattices and Wannier–Stark effects

We experimentally investigated several weak-barrier SLs (see also [7–9]). Below we present the results for two $GaAs/Al_xGa_{1-x}As$ superlattices, with periods $d = 196$ Å (SL426: 181-Å well, 15-Å barrier, number of periods $N = 100$) and 181 Å (SL816: 160-Å well, 20-Å barrier, number of periods $N = 1000$). In the absence of electric field the SL electron spectrum is a set of minibands (see Table 1 for the parameters). The Al content in both superlattices is $x =$ 10 % – 15 %. The SLs were not intentionally doped, and the electron concentration in them was $\sim 5 \times 10^{14}$ cm^{-3}. The SL period was determined from the X-ray diffraction data. To estimate the character of $I-U$ characteristics in weak-barrier SLs, we numerically simulated them by the Monte Carlo method using a simple quasi-classical model (see also [10]). Within this model the coherent processes – interminiband tunneling with a characteristic field F_t and Bragg reflections from the SL Brillouin zone boundaries – were considered as scattering ones. This approach ignores the phase relations for electrons performing the Bloch oscillations in different minibands. Apparently, this model yields an averaged (over the Wannier–Stark effects) $I-U$ characteristic. The results of simulation of the $I-U$ characteristics for the parameters corresponding to SL816 at the elastic scattering frequency $\nu_I = 10^{12}$ s^{-1} are shown in Fig. 2.

In weak fields ($F \ll F_t$), when the interminiband tunneling is insignificant, and the transport occurs within one miniband, the $I-U$ characteristic contains a descending portion (as in the case considered in [3]). This field range was discussed in detail in [9]. In fields with a strength $F \approx (0.3 - 0.5)F_t$ the current begins to monotonically rise due to the rise in the interminiband tunneling. This process is accompanied by a sublinear increase in the average electron energy (i.e., electron temperature) and enhanced scattering by optical phonons due to the injection of electrons into the second and higher minibands. The experimental $I-U$ characteristics (Fig. 3; see [8, 9] for measurement details) exhibit regular features (shoulders) in the ascending portion, which are repeated at voltages $U \sim 35N/(en)$ meV ($n = 4, 3, 2, \ldots$).

The shoulders are more pronounced for the voltage dependence of the derivative of $I-U$ characteristic with respect to electric field, dI/dU (see below).

We attribute the observed regular features, which manifest themselves against the background of exponentially rising nonresonant Zener current (which is qualitatively described by the results of the Monte Carlo simulation of the $I-U$ characteristic), to the resonant electron tunneling between Wannier–Stark levels belonging to different ladders and centred at quantum wells separated by several SL periods. To confirm this interpretation, we compared the positions of the features in the $I-U$ derivative with respect to the field with the calculated values of electric fields corresponding to the intersections (anti-

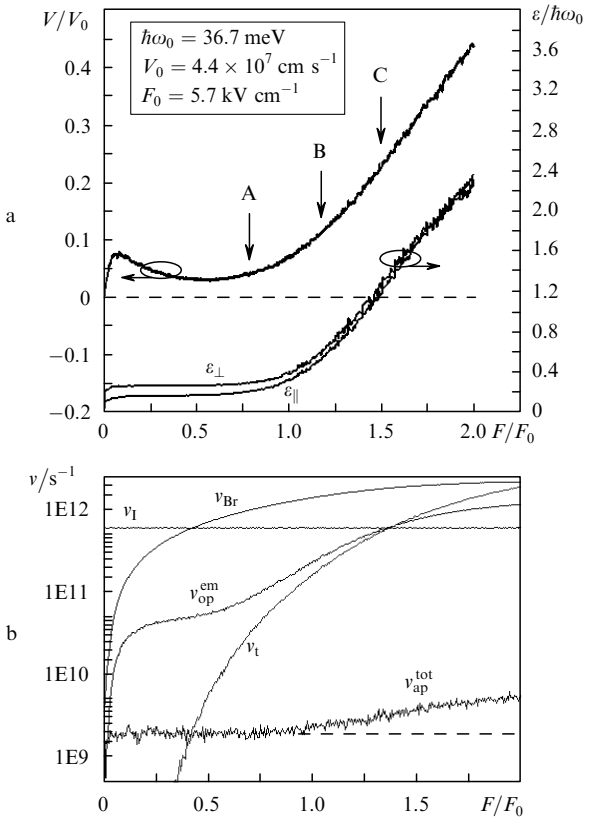

Figure 2. Results of the Monte Carlo simulation of the electron transport in SL816: (a) $V(F)$ is the average electron velocity and $\varepsilon_\parallel$ and $\varepsilon_\perp$ are, respectively, the average longitudinal and transverse electron energies; (b) ν_{op} is the scattering frequency by longitudinal optical phonon emission, ν_{ap} is the total scattering frequency by acoustic phonons, ν_I is the interface scattering frequency, ν_{Br} is the frequency of Bragg reflections from the edge of the Brillouin zone, ν_t is the electron tunneling frequency, and $\hbar\omega_0$ is optical phonon energy. The positions of the shoulders (which are due to the Wannier–Stark quantisation) in the experimental $I-U$ characteristics are indicated by arrows A, B, and C.

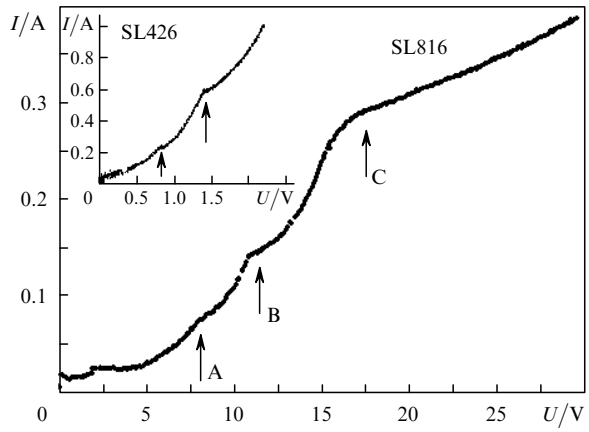

Figure 3. $I-U$ characteristics of SL816 and SL426. The hypothetical ranges of THz amplification are located near the shoulders in the $I-U$ characteristics – tunneling resonances between Wannier–Stark levels 1–2(4) (A), 1–2(3) (B), and 1–2(2) (C) (see Section 3 for the designations of resonances).

crossings) of Wannier–Stark levels belonging to different ladders (Fig. 4; see also [8]). The fan-shaped diagram (Fig. 4) indicates that the sets of anticrossings (vertical arrows A, B, and C) of the calculated Wannier–Stark levels fall in the intervals between the maxima and minima of the derivative of $I-U$ characteristic. For example, the feature in the $I-U$ curve near the energy $eFd \approx 12.5$ meV, which corresponds to the group-B anticrossings, is due to the electron resonant tunneling between the levels of the first, second, and third minibands. Note that the transitions between the first and second minibands occur through two wells to the third one [1–2 (3)], the transitions between the levels of the second and third minibands are through four wells to the fifth one [2–3 (5)], and the transitions between the levels of the first and third minibands are through seven wells to the eighth one [1–3 (8)]. The situation for A-group anticrossings is similar. The only difference is that the electron tunneling path includes more periods in this case: 1–2(4), 2–3(7), and 1–3(11), respectively. The far-range electron tunneling in weak-barrier SLs, obtained by comparing the calculated anticrossings and the features in the $I-U$ characteristic is a manifestation of strong delocalisation of the electron wave functions over several periods in electric field. Such a delocalisation provides a large dipole moment of the electron transition between Wannier–Stark ladders and a high gain at interladder transitions.

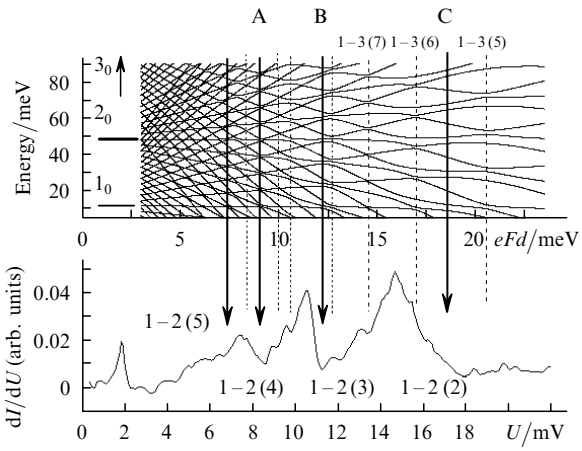

Figure 4. Calculated dependences of the positions of Wannier–Stark levels on electric field (top) and the first derivative of the $I-U$ characteristic of SL816 (bottom). The arrows combine the anticrossings of the 1–2(n) levels and the vertical dashed lines combine the anticrossings of the 1–3(n) levels.

3. Gain calculation

Figure 5 shows the SL potential profile in a dc electric field at a voltage somewhat exceeding that near the anticrossings of group B, which corresponds to the resonance between the first level (1) in the nth quantum well and the second level (2) in the $(n+3)$th well [1–2(3)]. When the electrons localised (centred) at the nth well of the first Wannier–Stark ladder interact with electromagnetic radiation, they can absorb quanta $\hbar\omega_1$ or $\hbar\omega_2$ to rise to the levels of the second Wannier–Stark ladder, localised in the $(n+1)$th or $(n+2)$th quantum wells, or emit a quantum $\hbar\omega_3$ to descend to the levels of the second ladder in the $(n+3)$th well. Obviously, the downward transitions to the second-ladder level localised in the $(n+4)$th, etc. wells may also occur. However, their frequency is relatively high in comparison with the frequencies ω_2 and ω_3, and we will disregard these

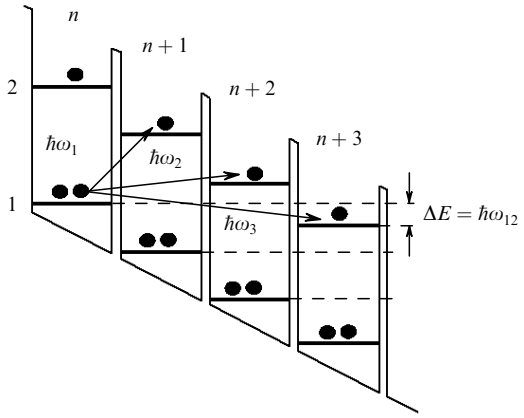

Figure 5. SL potential profile in a dc electric field F at a voltage slightly exceeding the value corresponding to resonance B and the transitions with absorption ($\hbar\omega_1$, $\hbar\omega_2$) and amplification ($\hbar\omega_3$).

transitions, as well as the upward transitions from levels of the first Wannier–Stark ladder in the nth well to levels of the second ladder in the $(n+1)$th well. Obviously, the upward (backward) transitions will be negelected for the same reason (relatively high transition frequency).

It follows from (1) that the energy of the jth Wannier–Stark level in the $(l+n)$th well is $\varepsilon_{j,l+n} = \varepsilon_{j,0} \pm (l+n)eFd$. The frequency of the transition between a level of the first ladder in the nth well and a level of the second ladder, spaced by n periods from the first one, is $\omega_n = (\varepsilon_{1,l+n} - \varepsilon_{2,l})/\hbar = (neFd - \Delta)/\hbar$, where $n = 3$ and 2 for the 1–2(3) (B) and 1–2(2) (C) transitions, respectively, and $\Delta = \varepsilon_{20} - \varepsilon_{10}$. In the SL816 sublattice, the gap Δ between the Wannier–Stark levels of the first and second ladders, localised in the same well, slightly exceeds the optical phonon energy $\hbar\omega_0 \approx 37$ eV (Table 1). Therefore, in moderate electric fields the population of the second level in the well (i.e., the population of the second Wannier–Stark ladder) is much lower than that of the first level (i.e., the first-ladder levels). In this case, the transitions between the levels of the nth and $(n+2)$th wells in Fig. 5 are not inverted and correspond to absorption, whereas the transition between the levels of the nth and $(n+3)$th wells is inverted and corresponds to amplification.

The population ratio for the ladder levels is the ratio of level populations n_1 and n_2 in a well. On the assumption that the electron distribution over well levels in the direction transverse to the SL axis is in equilibrium with the transverse electron temperature $T_{e\perp}$, we find the population ratio to be $n_2/n_1 = \chi = \exp(-\Delta/kT_{e\perp})$. To make estimates, one can equate the temperature $T_{e\perp}$ to the electron energy $\varepsilon_\perp$ in the direction transverse to the SL axis, calculated by the Monte Carlo method (Fig. 2). For the fields corresponding to the situation shown in Fig. 5, $T_{e\perp} \approx 100$ K. As a result, the ratio of the populations of the Wannier–Stark levels in the second (n_2) and first (n_1) ladders is $\chi \approx \exp(-4) \ll 1$. Thus, when calculating the gain and absorption for this case, we can approximately assume the second Wannier–Stark ladder to be unoccupied. The gain/absorption coefficient α_l of an electromagnetic wave polarised across the SL layers, in the case of transitions between ladder levels, can be written in the standard form, assuming that each transition occurs in a two-level system (see, for example, [12]). To calculate the gain (absorption) coefficient at each transition with a change in the well number by l periods, one has to know the matrix element Z of the coordinate along the SL growth direction for this transition; the relative difference in the ladder level populations, $\Delta n = (n_1 - n_2)$, $(n_1 + n_2) = 1$; the total electron density n_0 (in cm^{-2}) in the wells; the linear number of wells N_w (in cm^{-1}); and the transition broadening (collision frequency) ν. As a result, the expression for the gain (absorption) coefficient can be written as

$$\alpha_l = \frac{4\pi\sigma}{c\sqrt{\tilde{\varepsilon}_0}} = \frac{4\pi e^2 N_w n_0 \Delta n f}{2mc\sqrt{\tilde{\varepsilon}_0}} \frac{\nu}{(\omega - \omega_k)^2 + \nu^2}$$

$$= \frac{2\pi e^2 N_0 \Delta n f}{mc\sqrt{\tilde{\varepsilon}_0}} \frac{\nu}{(\omega - \omega_k)^2 + \nu^2}. \qquad (2)$$

Here, σ is the bulk negative conductivity; $\tilde{\varepsilon}_0$ is the SL permittivity; N_0 is the bulk electron concentration; $\Delta n = (1-\chi)/(1+\chi)$ is the relative difference in the level populations for the first and second Wannier–Stark ladders; ω_k is the transition frequency; m is the effective mass; and c is the speed of light. Within the approximation of electron temperature in the wells, as was discussed above, $\chi = \exp(-\Delta/kT_{e\perp})$. The transition frequency ω_k depends on the applied voltage. The 'oscillator strength' $f_l = 2mZ_l^2\omega_k/\hbar$ of the transition between the levels is determined by the coordinate matrix element $Z_l(F) = \int \psi_i(z,F) \times z\psi^*_{i+l}(z,F)\mathrm{d}z$, where $\psi_i(z,F)$, $\psi_{i+l}(z,F)$ are the electron wave functions. Note that in the weak-barrier SLs under consideration, where electrons can tunnel between wells separated by few periods, the coordinate matrix element near resonances may significantly exceed the SL period. In the case of detuning from resonance, the matrix element somewhat decreases but remains fairly large due to the barrier weakness. This can be seen in Fig. 6, which presents the field dependence of the matrix element Z_{ij}, obtained by calculating the Wannier–Stark wave functions for the SL816 structure. Note that these calculations were performed taking into account only two minibands: two levels in the wells {the calculation of the same matrix elements with allowance for three minibands (three levels) was reported in [7]}.

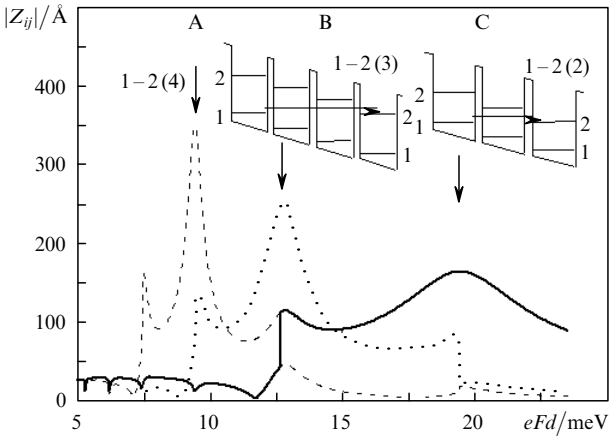

Figure 6. Calculated dependence of the matrix elements Z_{ij} on the electric field energy. The dashed (A), dotted (B), and solid (C) curves correspond to the 1–2(4), 1–2(3), and 1–2(2) transitions, respectively. A, B, and C are the resonant transitions between the first and second Wannier–Stark levels located in quantum wells spaced by 4, 3, and 2 periods, respectively.

Then we will consider two groups of transitions near anticrossings B and C [1–2(3) and 1–2(2), respectively]. We disregard other possible transitions because they either have a small matrix element [for example, the 1–2(4) transitions] or their frequencies significantly differ [for example, the 1–2(1) transitions]. In this case, the expression for the total gain/absorption coefficient at a change in energy eFd near resonances B and C can be written as

$$\alpha = \alpha_{1-2(3)} + \alpha_{1-2(2)} = \alpha_3 + \alpha_2,$$

where

$$\alpha_{2,3} = \frac{2\pi e^2 N_0 \Delta n f_{2,3}}{mc\sqrt{\tilde{\varepsilon}_0}} \frac{v}{(\omega_{2,3} - \omega)^2 + v^2}. \quad (3)$$

In these expressions $\Delta n \neq 1$, because at fields in the vicinity of resonances B and C the electron temperature is approximately equal to the optical phonon energy. Having determined the transverse energy from the calculations presented in Fig. 2, we find that $\Delta n \approx 2/3$ and $1/3$ for resonances B and C, respectively. The frequencies ω_2 and ω_3 are linear functions of the energy (field): $\hbar\omega_3 = 3eFd - \Delta$ and $\hbar\omega_2 = 2eFd - \Delta$. The oscillator strengths for these transitions are field functions, expressed in terms of the frequencies and matrix elements: $f_{2,3} = 2mZ_{2,3}^2\omega_{2,3}/\hbar$. As was noted above, at $eFd > \Delta/3$ (or at $eFd < \Delta/3$) the frequency $\omega_3 > 0$ ($\omega_3 < 0$) and the oscillator strength $f_3 > 0$ ($f_3 < 0$), which means amplification (absorption) on transition B. Similarly, at $eFd > \Delta/2$, $\omega_2 > 0$ and $f_2 > 0$, we obtain amplification on transition C; in the intermediate fields $\Delta/3 < eFd < \Delta/2$, depending on the matrix element Z_k, radiation can be either amplified or absorbed. With due regard to the above-reported Δn values, the gain takes the form

$$\alpha = \frac{2\pi e^2 N_0}{mvc\sqrt{\tilde{\varepsilon}_0}} \left[\frac{2}{3} \frac{f_2 v^2}{(\omega_2 - \omega)^2 + v^2} + \frac{1}{3} \frac{f_3 v^2}{(\omega_3 - \omega)^2 + v^2} \right] \quad (4)$$

(here the signs are chosen so as to provide amplification at $\alpha > 0$).

Figure 7 shows several gain spectra for superlattice SL816, calculated based on the matrix element (see Fig. 6), at electric fields near resonances B and C. At the electron concentration $N_0 = 10^{16}$ cm^{-3} and the effective scattering frequency $v = 5 \times 10^{12}$ s^{-1} in the SL the gain at the frequencies $\omega/2\pi \sim 10^{12} - 10^{13}$ s^{-1} can be as high as several hundreds of inverse centimeters.

The scattering frequency $v = 5 \times 10^{12}$ s^{-1}, which was used to estimate the amplification (this frequency may be somewhat overestimated), takes into account the scattering by optical phonons (their emission) at the second Wannier–Stark level in the wells. Note that the SLs under study had an electron concentration of $\sim 5 \times 10^{14}$ cm^{-3}, and at $v \sim 10^{13}$ s^{-1} the gain α at the 1–2(3) transitions was 20 cm^{-1}, which is apparently insufficient (see below) for amplification (lasing) in our experiment on the n^+–SL–n^+ stripe system.

4. Stripe cavities for Wannier–Stark oscillators

The choice of an appropriate cavity system played a key role in the design of THz cascade lasers. Currently, such lasers use cavities of two types, based on stripe lines [13].

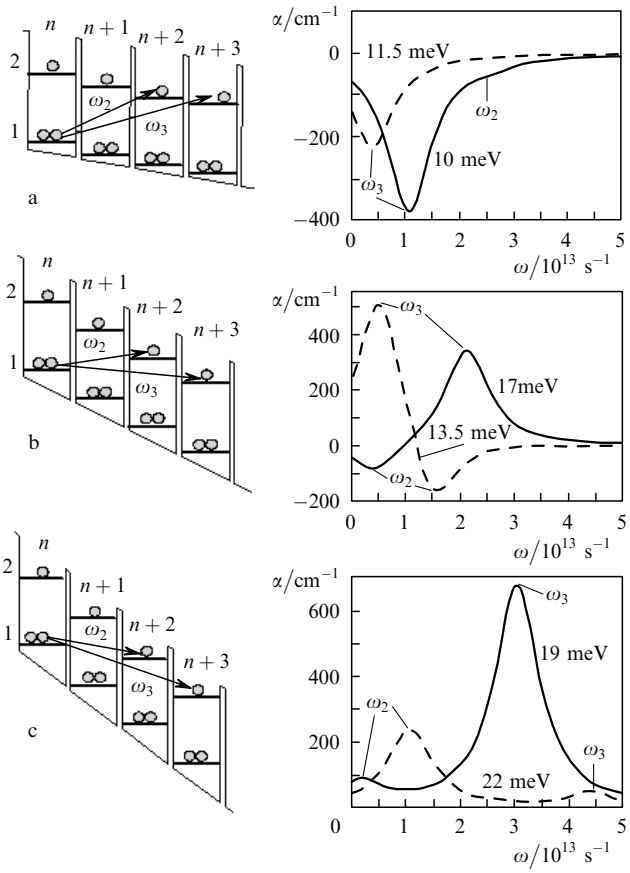

Figure 7. Gain and absorption spectra taking into account the 1–2(3) and 1–2(2) transitions in different fields F (a) to the left from resonance B at $eFd < \Delta/3$, (b) between resonances B and C at $\Delta/3 < eFd < \Delta/2$, and (c) to the right from resonance C at $eFd > \Delta/2$. The electron energies eFd and transition frequencies in the field F are indicated in the spectral lines; $N_0 = 10^{16}$ cm^{-3}, $v = 5 \times 10^{12}$ s^{-1}.

One of them, which was applied in the first cascade THz lasers [5], actually involves a weakly decaying symmetric TM plasmon in a thin, heavily doped layer (which served also as the bottom contact). The plasmon field penetrates into the insulating substrate, while at the other side of the doped layer, which closed the system of cascades (active region), the plasmon decayed at the metal contact. In the second-type cavities [14, 15] the active region was between two metal contacts. This configuration was obtained using a fairly complex technique: a structure with cascades and a deposited metal contact was 'welded' to another substrate with a metal, after which the initial substrate was etched off, and the second metal contact was deposited. The stripe loss is small for the first-type cavity; however, its filling factor by the active medium is small as well. At the same time, the volume occupied by the mode field is rather large, and one can obtain an acceptable output lasing diagram. The second approach is fairly expensive. At the same time, simple stripe structures with an active region (SL) between two heavily doped n^+ layers are not used in practice, because the gain of cascade THz lasers is insufficiently high, and many cascades are necessary to overcome the losses in the terminal layers of the structure. For a laser based on transitions between Wannier–Stark ladders, which is considered here, the gain at $N_0 = 10^{16}$ cm^{-3} can be higher than in cascade lasers, and one can use a stripe with n^+ terminal layers. Let us estimate the ohmic losses in the

$n^+ - n^+$ stripe cavity (Fig. 8) to determine the SL thickness required for laser operation. The absorption coefficient of electromagnetic radiation in both n^+ layers is $\alpha_s = 2S_1/(d_s S_0)$, where

$$S_0 = \frac{cEH}{8\pi} = \frac{cH^2}{8\pi\sqrt{\tilde{\varepsilon}_0}},$$
$$S_1 = \frac{cE_\tau H}{8\pi} = \frac{cH^2 \mathrm{Re} Z}{8\pi} = cH^2 \mathrm{Re}\,\frac{1}{\sqrt{\tilde{\varepsilon}}} \quad (5)$$

are the moduli of Poynting vectors (see Fig. 8);

$$\tilde{\varepsilon} \approx \tilde{\varepsilon}_0 - \frac{\omega_p^2}{\omega(\omega - i\tilde{\nu})} \approx -\frac{\omega_p^2}{\omega^2(1 - i\tilde{\nu}/\omega)} \quad (6)$$

is the permittivity in n^+ stripes; d_s is the distance between the plates; ω_p is the plasma frequency; and $\tilde{\nu}$ is the scattering frequency in n^+ stripes. At $\tilde{\nu} \ll \omega$ we have $\mathrm{Re}(1/\sqrt{\tilde{\varepsilon}}) \approx \tilde{\nu}/(2\omega_p)$. In this case, for the two n^+ terminal layers the absorption coefficient in the $n^+ - n^+$ stripe waveguide is

$$\alpha_s = \frac{\tilde{\nu}\sqrt{\tilde{\varepsilon}_0}}{\omega_p d_s}. \quad (7)$$

For GaAs ($\tilde{\nu} = 1.2 \times 10^{13}$ s^{-1} at the mobility $\mu = 2000$ cm^2 V^{-1} s^{-1}), doped to a level $N_0 \sim 10^{19}$ cm^{-3}, in the limit under consideration ($\tilde{\nu} \ll \omega$), the absorption coefficient is frequency-independent and amounts to 33 cm^{-1} for $d_s =$ 18 μm. In the case of a stripe with one terminal layer (n^+–metal) the absorption is lower by a factor of 2 (~ 16 cm^{-1}). Note that these loss estimates are in agreement with the absorption coefficient value $\alpha_s = 50$ cm^{-1}, which was measured in [14] for a $n^+ - n - n^+$ structure at $d_s =$ 10 μm and $N_0 = 5 \times 10^{18}$ cm^{-3}.

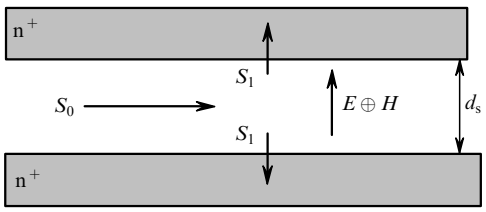

Figure 8. Stripe cavity.

Thus, this loss in the $n^+ - SL - n^+$ structure is much less than the above-reported gain for the transitions between Wannier–Stark ladders at an SL doping level $N_0 \geqslant 10^{15}$ cm^{-3}. Hence, such stripe cavities can be used to design the Wannier–Stark lasers considered here.

5. Conclusions

We investigated the possibility of amplifying THz radiation based on the universal mechanism of inversion between Wannier–Stark ladders in weak-barrier SLs. The THz gain spectra were obtained by calculating the wave functions and matrix elements of optical transitions in a dc electric field. It was established that the matrix elements of some transitions in these SLs are fairly large, and the gain obtained greatly exceeds the values typical of quantum cascade lasers. The estimated gain in the Wannier–Stark scheme and ohmic losses in a $n^+ - SL - n^+$ stripe waveguide give grounds to expect amplification in SLs 10–15 μm thick at a temperature of 4–77 K in the long-wavelength THz range ($\lambda =$ 200 – 250 μm) at dopant concentrations $N_0 \geqslant (1 - 5) \times 10^{15}$ cm^{-3}.

On the whole, we believe that the approach to intraband lasers based on SLs with narrow barriers may have a wider range of application. It apparently can be used for n-type Ge–Si superlattices grown on relaxed silicon substrates in the [111] direction, where all electronic valleys are equivalent (see the discussion of cascade lasers based on this system [16, 17]). We expect the use of weak barriers (with a low germanium content) within this approach to make it possible to obtain fairly thick SLs of high structural quality on this material. At the same time, for weak-barrier GaAs/AlGaAs SLs, it would be of interest to investigate the case of shorter periods with transitions between Wannier–Stark ladders in the mid-IR range.

Acknowledgements. We are grateful to Yu.N. Drozdov for the detailed X-ray diffraction study and to M.N. Drozdov for the Auger analysis of the SLs. This study was supported by the program 'Basic Research in Nanotechnology and Nanomaterials' of the Presidium of the Russian Academy of Sciences (Grant No. 27), Russian Foundation for Basic Research (Grant No. 09-02-00380-a), and Grant NSh-2786.2008.2 of the President of the Russian Federation for Support of Leading Scientific Schools.

References

1. Kazarinov R.F. and Suris R.A. *Fiz. Tekh. Poluprovodn.*, **5**, 797 (1971) [*Sov. Phys. Semicond.*, **5**, 707 (1971)].
2. Kazarinov R.F. and Suris R.A. *Fiz. Tekh. Poluprovodn.*, **6**, 148 (1972) [*Sov. Phys. Semicond.*, **6**, 120 (1972)].
3. Esaki L., Tsu R. *IBM J. Res. Dev.*, **14**, 61 (1970).
4. Faist J., Capasso F., Sivco D. L., et al. *Science*, **264**, 553 (1994).
5. Kohler R., Tredicucci A., Beltram F., et al. *Nature*, **417**, 156 (2002).
6. Faist J. et al. *IEEE J. Quantum Electron.*, **38**, 533 (2002).
7. Andronov A.A., Dodin E.P., Nozdrin Yu.N., Zinchenko D.I. *Phys. Stat. Sol. C*, **5**, 190 (2008).
8. Andronov A.A., Dodin E.P., et al. *Fiz. Tekh. Poluprovodn.*, **43**, 240 (2009) [*Semicond.*, **43**, 228 (2009)].
9. Andronov A.A., Dodin E.P., et al. *Fiz. Tekh. Poluprovodn.*, **43**, 248 (2009) [*Semicond.*, **43**, 236 (2009)].
10. Andronov A.A., Nefedov I.M., Sosnin A.V. *Fiz. Tekh. Poluprovodn.*, **37**, 378 (2003) [*Semicond.*, **37**, 360 (2003)].
11. Willenberg H., Dohler G.H., Faist J. *Phys. Rev. B*, **67**, 085315 (2003).
12. Yariv A. *Introduction to Optical Electronics* (New York: Holt, Rinehart, and Winston, 1971; Moscow: Vysshaya shkola, 1983).
13. Williams B.S., Kumar S., et al. *Appl. Phys. Lett.*, **83** (11), 2124 (2003).
14. Rochat M. et al. *Appl. Phys.Lett.*, **78** (14), 1967 (2001).
15. Kohen S., Williams B.S., Hu Q. *J. Appl. Phys.*, **97**, 053106 (2005).
16. Lever L., Valavanis A., et al. *Appl. Phys. Lett.*, **92**, 021124 (2008).
17. Valavanis A., Lever L., et al. *Phys. Rev. B*, **78**, 035420 (2008).